# Parameterized Electrostatic Gap Models for Structured Design of Microelectromechanical Systems

Michael S.-C. Lu* and Gary K. Fedder*†

*Department of Electrical and Computer Engineering, and *†The Robotics Institute
Carnegie Mellon University, Pittsburgh, PA, USA, [mslu, fedder]@ece.cmu.edu

## ABSTRACT

Electrostatic gap models for hierarchical MEMS circuit design are studied and parameterized through a series of finite element simulations and mathematical modeling. The models take into account the fringing fields which contribute large capacitances in low-aspect-ratio surface-micromachined devices. Angular orientation of electrode sidewall is taken into account to accommodate simulation of manufacturing variations. Results show that capacitances reconstructed from these models deviate from the original data by less than 5% on the average. Simulations on cantilever beam actuators show comparable results between the MEMS hierarchical circuit analysis and the electromechanical finite element analysis. Experimentally, less than 7% error in the pull-in voltages is obtained by considering the sidewall angle.

***Keywords***: MEMS, parameterization, capacitance, comb finger, structured design.

## INTRODUCTION

In order to design complex microelectromechanical systems having a large numbers of multi-domain components, a hierarchically structured design approach has been reported [1][2]. The approach adopts the notion of nodal simulation, which is the same concept used for analog circuit simulation. At the lowest level in the design hierarchy, MEMS components are represented as interconnected combinations of atomic behavioral models, and solved in a mixed-mode simulator. The set of low-level elements includes beams, plates, anchors, and gaps. Models for beams and plates with geometric parameters are described in [1].

In this paper, we focus on the modeling of electrostatic gaps (*i.e.*, capacitances and forces) for design of MEMS devices using the hierarchical design approach. Most electrostatic microactuators are composed of a small set of gap geometries. A capacitance macromodel on a fixed-geometry accelerometer has been reported [3], in terms of in-plane and out-of-plane spatial coordinates but without parameterization of the geometry. Parameterized models of comb fingers with rectangular cross-section have been derived using a conformal mapping method by Johnson and Warne [4]. In the low-level MEMS circuit schematic, electrostatic gap elements are interconnected with beam and plate elements to allow representation of most MEMS devices. By generating a set of gap models having geometric parameters, these MEMS circuit schematics can be simulated without resorting to intermediate modeling.

In cases where the aspect ratio of these devices is low, fringing capacitances become significant and need to be characterized in order to better simulate the electromechanical behavior of the devices. To deal with a wide range of geometry in designs, the gap model is parameterized in terms of electrode dimensions and separation. The geometry is either assigned by designers directly in a schematic simulation, or extracted from the mask-level layout. Similar effort on parameterized capacitances is performed for time delay estimation for VLSI interconnect [5], where an analytic formula of interconnect capacitance is preferred over time-consuming numerical simulation.

## GAP MODELING

Models of two electrodes as shown in Figure 1(a) and 1(b), and comb fingers in Figure 1(c) are characterized. Figure 1(a) features two electrodes of the same width, while the geometry in Figure 1(b) has a single, much wider electrode. Variations of gap separation ($g$), thickness ($h$), width ($w$) and angular sidewall slope ($\theta$) induced from the manufacturing process are taken into account in the models. The geome-

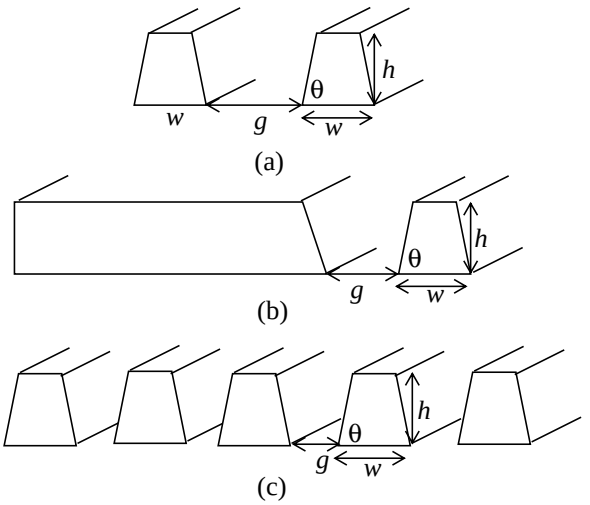


Figure 1: The geometries studied for gap modeling. (a) Two electrodes of the same width. (b) One electrode much wider than the other. (c) Comb-finger array.

tries studied do not include an underlying ground plane. However, the modeling approach is extendable to such actuators.

No exact analytical solutions have been derived to take sloped sidewalls into account by the conventional conformal mapping method. To make gap models accurate, numerical data produced from finite element simulation [6] are analyzed by least-squares fits. The capacitance equation used in fitting is:

$$C = \frac{\varepsilon_o h}{g}\left(K_1\left(\frac{w}{h},\theta\right) + \frac{g}{\pi h}\left(K_2\left(\frac{w}{h},\theta\right) + K_3\left(\frac{w}{h},\theta\right)\ln\left(\frac{\pi h}{g}\right)\right)\right) \quad (1)$$

which has a physical basis as the analytical equation derived for a zero-thickness plate on top of an infinite ground plane [7]. Capacitance depends on the ratios of electrode dimensions and separations, where $C$ is capacitance per unit length, and $\varepsilon_o$ is the permittivity of air.

The coefficient functions $K_i$ are functions of the cross-sectional geometry. These functions are first obtained for every $\left(\frac{w}{h},\theta\right)$ pair by curve-fitting its corresponding $C$ vector with respect to the $g/h$ ratio. Then a surface fit on $w/h$ and $\theta$ gives the final coefficient functions.

As an example, values of capacitance per unit length for two electrodes of the same width are shown in Figure 2 for $w/h \in [0.5, 5]$, $g/h \in [0.1, 3]$ and $\theta \in [1.32582, \pi/2]$ (in radians).

Each $\left(\frac{w}{h},\theta\right)$ pair has a corresponding capacitance curve drawn with respect to $g/h$ in the mesh. $K_i$ values for each are obtained by curve-fitting the capacitance equation, as plotted in Figure 3. Non-physical basis functions are chosen out of the set $(w/h)^{\alpha}$, $\theta^{\beta}$, $\ln(w/h)$, $\ln(\theta)$, $e^{(w/h)}$, $e^{\theta}$, and out of products of these functions. The final coefficient functions listed below are obtained through another surface fit.

$$K_1 = -1.565 + 0.2818\left(\frac{w}{h}\right)^{-0.04348} - 2.986\theta^{5.9} + 0.4446e^{\theta}\theta^{6.002} + 28.87\ln(\theta) \quad (2)$$

$$K_2 = 21.43 - 15.5\left(\frac{w}{h}\right)^{-0.02146} - 10.07e^{\theta}\left(\frac{w}{h}\right)^{-0.03944}\theta^{-1.877} + 23.7\theta^{0.09913} + 0.0484e^{\left(\frac{w}{h}\right)}\theta^{0.8278}\left(\frac{w}{h}\right)^{-2.244} - 13.6\ln(\theta) \quad (3)$$

$$K_3 = 10.86 - 1.512\left(\frac{w}{h}\right)^{-0.2517} - 0.007964\theta^{15.31} + 0.005087\ln\left(\frac{w}{h}\right) - 62.71\ln(\theta) + 20.05\theta^{2.529}\ln(\theta)\left(\frac{w}{h}\right)^{-0.002656} \quad (4)$$

Using the same procedure for the case where one electrode is much wider than the other, the coefficient functions are:

$$K_1 = -1.353 - 2.827\theta^{5.988} + 0.4272e^{\theta}\theta^{6.076} - 0.01112\ln\left(\frac{w}{h}\right) + 28.06\ln(\theta) \quad (5)$$

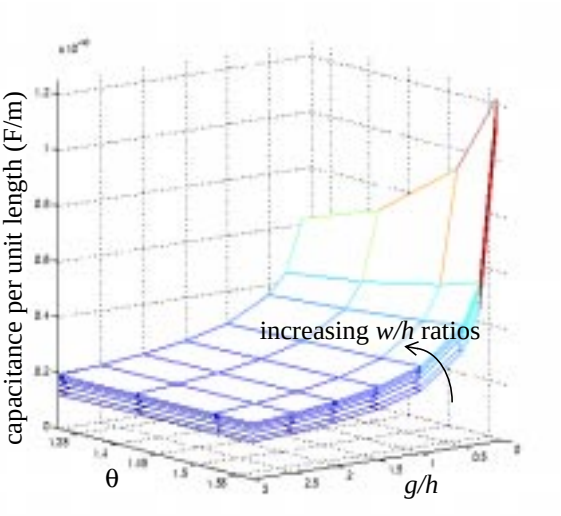


Figure 2: Capacitance per unit length as a function of $g/h$ and $\theta$ for two electrodes of the same width.

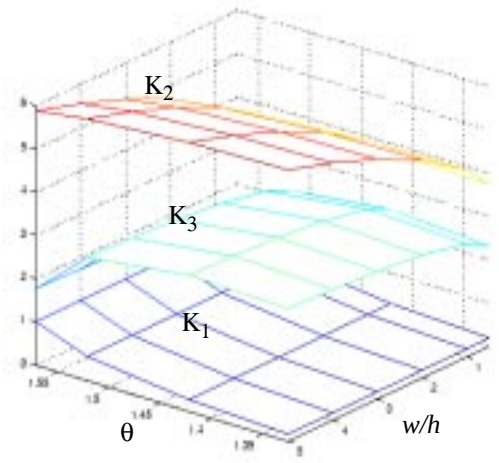


Figure 3: K's values drawn over $w/h$ and $\theta$.

$$K_2 = 2.058 - 0.1588\ln\left(\frac{w}{h}\right) - 0.2527\ln(\theta) + 30.9\left(\frac{w}{h}\right)^{0.2687}\ln(\theta) \quad (6)$$
$$\theta^{-3.177}$$

$$K_3 = 12.46 - 0.03697\theta^{12.79} + 0.3212\ln\left(\frac{w}{h}\right) - 109.4\ln(\theta) + 45.38\theta^{1.989}\ln(\theta)\left(\frac{w}{h}\right)^{-0.001315} \quad (7)$$

Gap models of comb fingers are constructed for fingers at the center and the edge. Finger capacitance gradually increases as it moves away from the center. The coefficient functions for comb fingers far away from the edge are:

$$K_1 = -1.441 - 0.0291\left(\frac{w}{h}\right)^{-0.3762} - 2.2239\theta^{6.254} + 0.3313e^{\theta}\theta^{6.412} + 25.28\ln(\theta) \quad (8)$$

$$K_2 = -9.466 + 12\left(\frac{w}{h}\right)^{-0.1935} - 1.137\times10^{-4}e^{\theta}\theta^{14.78} + 2.998\ln\left(\frac{w}{h}\right) \quad (9)$$
$$+ 0.08495\ln(\theta)$$

$$K_3 = 7.32 - 1.36\left(\frac{w}{h}\right)^{-0.2075} + 0.63\theta^{8.022} - 0.01269e^{\theta}\theta^{12.24} + \quad (10)$$
$$0.1648\ln\left(\frac{w}{h}\right) - 29.42\ln(\theta)$$

And coefficient functions for comb fingers at the edge are:

$$K_1 = -1.799 + 0.5043\left(\frac{w}{h}\right)^{-0.02533} - 2.97\theta^{5.918} + 0.4446e^{\theta}\theta^{6.013} \quad (11)$$
$$+ 28.83\ln(\theta)$$

$$K_2 = -0.4472 + 3.009\left(\frac{w}{h}\right)^{0.2986} + 0.03332e^{\theta}\theta^{1.226}\left(\frac{w}{h}\right)^{-0.7201} \quad (12)$$
$$- 3.385\times10^{-4}\theta^{16.02} - 0.04904\ln(\theta)$$

$$K_3 = 178.038 - 1.969\left(\frac{w}{h}\right)^{0.207} + 347.593e^{\theta}\left(\frac{w}{h}\right)^{0.001652}\theta^{14.847} \quad (13)$$
$$- 395.697\theta^{-4.252} - 263.609\ln(\theta)$$

Values of capacitance per unit length are recalculated from Eq. (1)-(13), and compared with the original data. For the case of two electrodes with the same width, it has an average deviation of 1.6% and a maximal deviation of 5.7%. The case with a single wider electrode has an average deviation of 1.4% and a maximal deviation of 4.9%. For comb fingers, center capacitance has an average deviation of 2.4% and a maximal deviation of 13.2%. The capacitance at the edge has an average deviation of 2.3% and a maximal deviation of 9.2%.

### Electrostatic Forces

In the nodal simulation, the gap model is connected to the nodes at the ends of two adjacent beam models. Values of capacitance and electrostatic forces are calculated by the separation, overlap, and beam dimensions. Force parallel to the beams, calculated as $F_{\|} = \frac{1}{2}CV^2$, is applied directly to the nodes. Distributed force per unit length $q$ of magnitude $\frac{1}{2}\frac{dC}{dg}V^2$ perpendicular to the beams is lumped at the nodes as $F_1$ and $F_2$ by the principle of conservation of force and moment, as shown in Figure 4. Thus, $F_1 = F_2 = ql/2$.

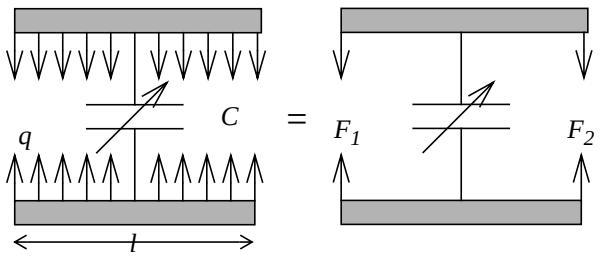


Figure 4: Decomposition of distributed electrostatic force into pointed forces.

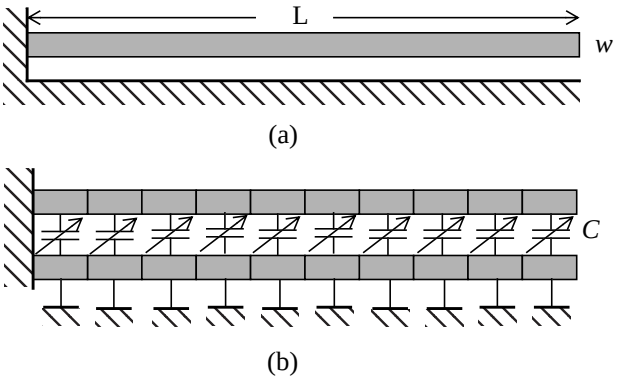


Figure 5: Cantilever beam actuator. (a) Geometry from the top view. (b) Represented as schematic of interconnected beams and gap models for nodal simulation.

## SIMULATION

The geometry and the schematic representation of the cantilever beam actuator is shown in Figure 5. A total of twenty beam instances (ten for stator and ten for beam) and ten gap instances are placed in the schematic for nodal simulation. Results of nodal simulation and finite element analysis [8] for pull-in voltage of the actuators with 2 μm width, 2 μm gap, and $\theta = \pi/2$ as function of beam length are plotted in Figure 6. A maximal -1.7% deviation of pull-in voltage from the finite element simulation is shown. Values of pull-in voltage in both simulations are inversely proportional the beam length squared.

A plot of tip displacement with respect to the applied voltage for a 100 μm long beam actuator is shown in Figure 7. Good agreement is shown except near the edge of snap-in. For one data point, it takes nodal simulation 1.7 seconds

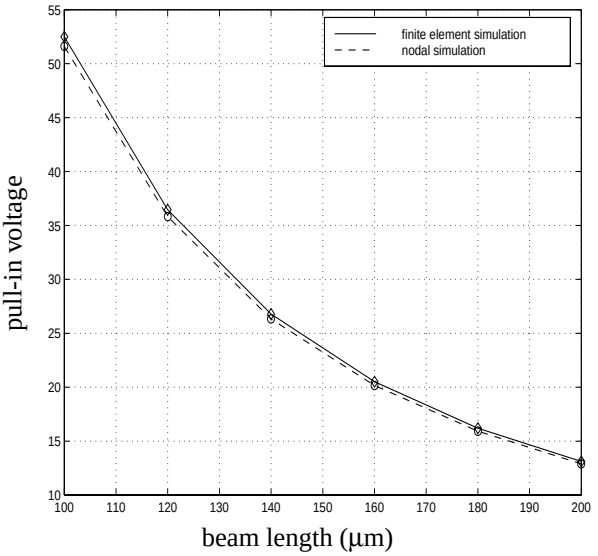


Figure 6: Nodal and finite element simulations of pull-in voltage.

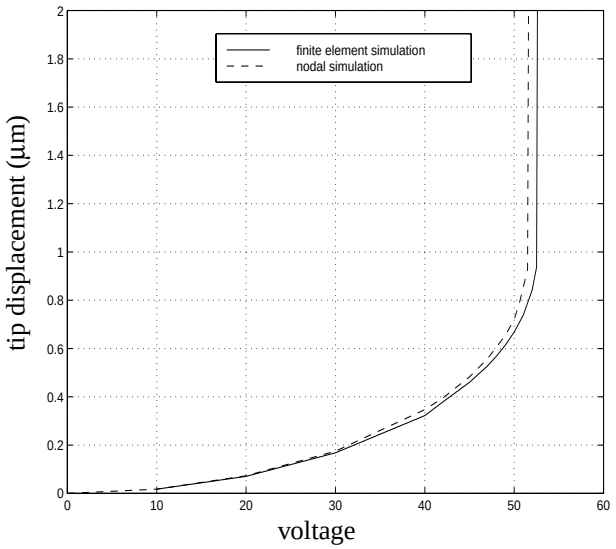


Figure 7: Comparison of tip displacement vs. applied voltage for a 100μm-long beam actuator.

(CPU time) on the average to complete, while finite element analysis take 280 seconds.

## EXPERIMENT

Pull-in voltages of beam actuators fabricated in the MUMPs process were measured. Actual beam cross-section and gap separation are taken into account in the nodal and finite element simulations ($h$ = 2 μm, $w$ = 1.7 μm, $g$ = 2.3 μm, and θ = 1.496 radians). Experimental values are significantly lower than the simulation results shown in Figure 6. Up to 25% error occurs if only nominal layout dimensions are considered in the simulation. The results are listed in Table 1.

**Table 1: Results of pull-in voltage from experiment, nodal and finite element simulations of polysilicon beams.**

| beam length (μm) | experiment (volt) | nodal simulation (volt) | finite element (volt) |
|---|---|---|---|
| 100 | 40.0 | 42.5 (+6.3%) | 44.2 (+10.5%) |
| 150 | 18.4 | 19.1 (+3.8%) | 19.7 (+7.1%) |
| 200 | 10.4 | 11.0 (+5.8%) | 11.1 (+6.7%) |

The capacitances between the ground plane and the electrodes are insensitive to the electrode separation. Therefore, the contribution of the electrostatic force from the ground plane can be neglected. Data shows that for θ = π/2, less than 3% deviation in force is shown by comparing our comb-finger model to Johnson's model with a ground plane.

## CONCLUSION

Parameterized gap models have been constructed with angular orientation taken into account to minimize the sensitivity to the manufacturing process. Less than average 5% error is shown by comparing with values from the original finite element simulation. By using gap models in the nodal simulation of cantilever beam actuators, results comparable to the electromechanical finite element analysis are obtained easily with shorter simulation time. Manufacturing variations are taken into account by varying appropriate sidewall parameters. Simulation results agree to within 7% of experimental data, demonstrating the ability of nodal analysis to predict behavior of distributed electrostatic systems.

## ACKNOWLEDGEMENT

This research effort is sponsored by the Defense Advanced Research Projects Agency (DARPA) and U. S. Air Force Research Laboratory, under agreement number F30602-96-2-0304. The U.S. Government is authorized to reproduce and distribute reprints for governmental purposes notwithstanding any copyright notation thereon. The views and conclusions contained herein are those of the authors and should not be interpreted as necessarily representing the official policies or endorsements, either expressed or implied, of DARPA, the U. S. Air Force Laboratory, or the U. S. Government.

## REFERENCES

[1]T. Mukherjee and G. K. Fedder, "Structured Design of Microelectromechanical Systems," in *Proc. of the 1997 Design Automation Conference*, Anaheim, CA, pp. 680-685, 1997.

[2]J.V. Clark, N. Zhou, K.S.J. Pister, "MEMS Simulation using SUGAR v0.5, "*Solid-State Sensor and Actuator Workshop*, Hilton Head, South Carolina, June 8-11, 1998.

[3]N. R. Swart, S. F. Bart, M. H. Zaman, M. Mariappan, J. R. Gilbert, and D. Murphy, "AutoMM: Automatic Generation of Dynamic Macromodels for MEMS Devices," in *Tech. Dig. IEEE Micro Electro Mech. Syst. Workshop*, Heidelberg, Germany, pp. 178-183, 1998.

[4]W. A. Johnson and L. K. Warne, "Electrophysics of Micromechanical Comb Actuators," *J. of Microelectromechanical Systems*, Vol. 4, No. 1, pp. 49 - 59, 1995.

[5]G. S. Samudra and H. L. Lee, "A Set of Analytic Formulas for Capacitance of VLSI Interconnects of Trapezium Shape," *IEEE Trans. on Electron Devices*, Vol. 41, No. 8, pp. 1467-1469, 1994.

[6]Maxwell 2D Field Simulator: User's Reference. Ansoft Corporation, June, 1994.

[7]H. B. Palmer, "The Capacitance of a Parallel-plate Capacitor by the Schwartz-Christoffel Transformation," E*lectrical Engineering* 56, pp. 363-366, March, 1937.

[8]Memcad 4.0. Microcosm Technologies, Inc., Cambridge, MA.